Regular Article

ANALYTICAL AND BIOANALYTICAL CHEMISTRY RESEARCH

Published by the Iranian Chemical Society

Anal. Bioanal. Chem. Res., Vol. 7, No. 1, 131-150, January 2020.

Synthesis of a Novel Magnetic Nanocomposite and its Application to the Efficient Preconcentration and Determination of Malachite Green in Fish Samples Using Response Surface Methodology

Masoud Shariati-Rad* and Narjes Haghparast

Department of Analytical Chemistry, Faculty of Chemistry, Razi University, Kermanshah, Iran

(Received 4 November 2018 Accepted 5 August 2019)

Malachite green (MG) has been extensively used as a fungicide and parasiticide in fish farms. At present, the use of MG in aquaculture is forbidden because MG and its metabolite were reported to cause human carcinomatosis and mutagenesis. Owing to its low cost and availability, MG may still be used. Herein, extraction and preconcentration methods were developed for spectrophotometric determination of trace amounts of MG in different samples. The methods are based on the extraction of dye by SiO_2 coated magnetic nanoparticles (Fe_3O_4@SiO_2) and chloropropyltriethoxysilane (CPTS) core-shell magnetic nanocomposite (Fe_3O_4@SiO_2-CPTS). The influence of pH, dosage of the adsorbent and contact time on the extraction of the dye was explored by response surface methodology. The calibration curve was linear in the range of 0.01-15.00 mg l^{-1} with detection limit of 2.0×10^{-4} mg l^{-1} by Fe_3O_4@SiO_2-CPTS. Extraction and preconcentration, based on the two magnetic nanoparticles, were successfully applied for determination of MG in various water and fish samples.

Keywords: Preconcentration, Malachite green, Magnetic nanocomposite, Response surface methodology, Fish sample

INTRODUCTION

Malachite green (MG), a triarylmethane dye ($C_{23}H_{25}ClN_2$), is a dark green cationic dye. This dye, like other triphenylemethanes, can exist in two ionic forms; *i.e.*, the dye salt and the carbinol or pseudobase [1]. I t acts as a pseudobase which enters cells due to its great lipid solubility [2]. More than eighty percent of the absorbed MG is converted metabolically to its reduced form, leucomalachite green (LMG) [3]. The chemical structure of MG is shown in Scheme 1.

MG has been extensively used as a topical fungicide [4,5] and parasiticide in fish farming throughout the world since 1936 [6]. The dye is highly effective against protozoal and fungal infections as well as skin and gill flukes, and therefore, it is extensively used as biocide in the aquaculture industries [7,8].

At present, the use of MG in aquaculture has become a matter of concern because MG and its metabolite were reported to cause human carcinomatosis and mutagenesis [9,1]. Thus, using MG in aquaculture has been forbidden in many countries. However, owing to low cost and availability, MG may still be used illegally.

The use of MG in veterinary medicinal products is not authorized in the European Commission and U.S., and also not approved in China [10,11]. The European minimum required performance limit, a quality parameter for residue laboratories, is set as the sum of MG and LMG at 2.00 µg kg^{-1} [12]. Consequently, it is of great importance that any related enforcement focuses on the determination of the lowest concentrations for both MG and LMG [13].

Nanoparticles (NPs) have been rapidly and extensively developed, and widely used in removal and extraction purposes [14-25]. NPs have a high ratio of surface area to

*Corresponding author. E-mail: mshariati_rad@yahoo.com

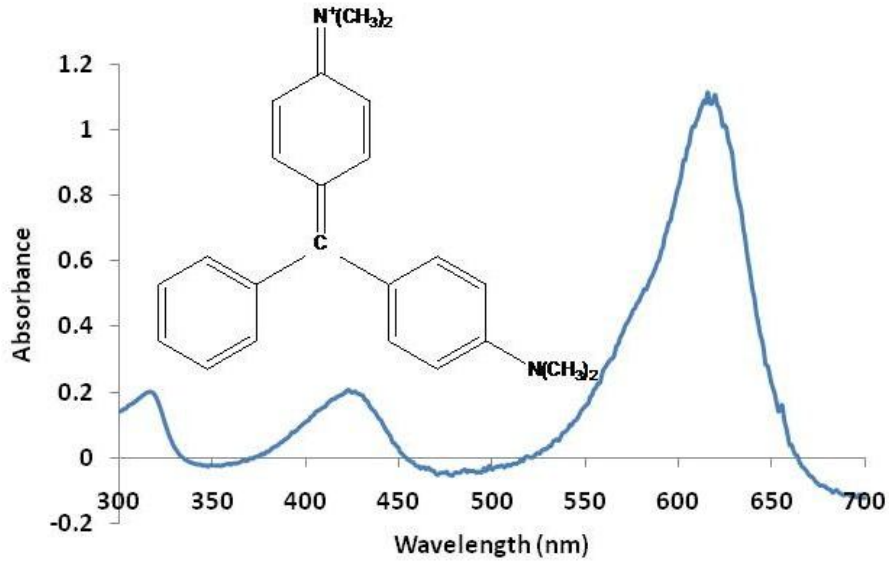

Scheme 1. Structural formula of MG and corresponding spectrum

volume providing a much greater extraction capacity and efficiency compared with other adsorbents. Moreover, the functional groups of the surface of NPs can be easily modified to achieve selective sample extraction. Since magnetic NPs (MNPs) are superparamagnetic, it is easy to separate them along with the adhered analytes from the aqueous solution or complicated matrices by simply applying an external magnetic field without any filtration or centrifugation. However, an unavoidable problem associated with MNPs is their intrinsic instability causing formation of agglomerates. Moreover, bare metallic nanoparticles are highly reactive, and are easily oxidized in air resulting in loss of magnetism and dispersibility. For many applications, it is thus crucial to develop protection strategies to chemically stabilize the bare MNPs. These strategies comprise grafting or coating with an inorganic layer, for example, silica or carbon, or coating with organic species including surfactants and polymers [26]. It is noteworthy that in many cases, the protecting shells not only stabilize the nanoparticles but are also used for further functionalization.

Methods including enzyme-linked immunosorbent assay (ELISA) [27-29], spectrophotometery [30], gas chromatography–mass spectrometry (GC-MS) [31], high performance liquid chromatography (HPLC) [3,32-36], and liquid chromatography-tandem mass spectrometry (LC-MS/MS) [37-39] have been reported for the detection of MG residues in different fish samples. Most of the methods mentioned are expensive, complex and time consuming. However, development of sensitive methods which are free from interferences is continuously needed. Therefore, extraction and preconcentration of MNPs-based MG were emerged [16,40,41].

In the present work, a novel functionalized MNP is introduced for extraction, preconcentration and determination of the very low amounts of MG in complex sample matrices. Conditions for the efficient adsorption and extraction of MG are explored by response surface methodology.

EXPERIMENTAL

Reagents and Materials

All of the chemicals and reagents used in this work were of analytical reagent grade. Hydrochloric acid, sodium dodecyl sulfate (SDS), acetic acid and MG were purchased from Merck (Merck, Darmstadt, Germany). Deionized water was used for preparation of the solutions throughout the study. The stock solutions (10.0 mg l^{-1} and 100.0 mg l^{-1}) of MG were prepared in deionized water. Moreover, 0.03 M solution of SDS in 0.1 M hydrochloric acid and pure acetic acid was used for desorption of dye from the MNPs.

For synthesis of MNPs, tetraethoxysilane (TEOS), $FeCl_3.6H_2O$, $FeCl_2.4H_2O$, ethanol (98%), ammonia (28%), chloropropyltriethoxysilane (CPTS) all from Merck (Merck, Darmstadt, Germany) were used as received.

Instrumentation and Software

Recording the absorption spectra in the spectral range of 200-800 nm was performed by an Agilent 8453 UV-Vis spectrophotometer equipped with diode array detector in 1 cm path length quartz cells. A JENWAY ion-meter, Model 3345, was used for pH adjustment. GLF-3005 shaker was used for shaking solutions containing MNPs. An ordinary magnet was used to separate MNPs from the solutions.

Design and analysis of the central composite experiments were carried out by the MINITAB (Minitab Inc. Release 16.0) statistical package.

A Philips X0 Pert (40 kV, 30 mA) X-ray diffractometer, using a Cu Kα radiation source (k = 1.541 Å) and a nickel filter in the 2θ range of 5.0º-99.8º with a step size of 0.4º, was used to record X-ray diffraction (XRD) pattern of the MNPs. The morphologies of the synthesized MNPs were observed by means of an EM-3200 scanning electron microscope (KYKY CO., China). For recording FTIR spectra, an Alpha FTIR spectrometer (Bruker, Germany) was employed.

Synthesis of SiO_2 Coated MNPs (Fe_3O_4@SiO_2) [42]

The SiO_2-coated MNPs were prepared using sol-gel method. Briefly, appropriate amounts of iron nitrate ($Fe(NO_3)_3.9H_2O$), tetra ethoxysilane (TEOS) and oxalic acid ($H_2C_2O_4.2H_2O$) were separately dissolved in ethanol. The three solutions were heated up to 50 °C and stirred for 20 min. The TEOS was added to the iron nitrate followed by oxalic acid addition under strong stirring at 60 °C for 2 h. The precipitate composed of iron oxalate and TEOS was progressively hydrolyzed by the hydration water of iron nitrate and mainly oxalic acid.

In the acidic condition (pH ≈ 1), the product of hydrolysis ($Si(OH)_4$) was condensed with other materials to a homogeneous gel. Then, the monolithic gel was dried at 110 °C in vacuum for 16 h. Finally, the dried powder was calcined (450 °C for 6 h) to produce solid magnetic composite.

Preparation of Fe_3O_4 Nanoparticles [42]

To a solution of $FeCl_3.6H_2O$ (2.7 g, 10 mmol) in 150 ml deionized water, $FeCl_2.4H_2O$ (1 g, 5 mmol) was added under nitrogen gas atmosphere. The resultant solution was stirred for 0.5 h in 80 °C. Then, ammonia (11.0 M) was added quickly with vigorous stirring to make a black solid product and the mixture was further stirred for 2 h in 80 °C and the black magnetite solid product was filtered and washed with ethanol three times and was then dried at 80 °C.

Immobilization of CPTS- SiO_2 onto Fe_3O_4 Core-shell Nanoparticles (Fe_3O_4@SiO_2-CPTS) [43]

An amount equivalent to 1 g of the synthesized Fe_3O_4 in the previous section was added to the mixture of 2 ml of tetraethoxysilane (TEOS) and 0.5 ml of CPTS. Then, after addition of 30 ml of ethanol and 1 ml of deionized water, 2 ml of ammonia was added dropwise during 30 min and stirred for 2 h at room temperature. Then, the product was separated by an external magnet and was washed three times by deionized water and ethanol and dried at 80 °C for 2 h (Fig. 1).

Analytical Procedure

Calibration curves were obtained by adding 10 and 100 ml of MG solutions with different concentrations in optimal pH to 13.0 mg of adsorbent Fe_3O_4@SiO_2 and 15.5 mg of Fe_3O_4@SiO_2-CPTS, respectively, in separate series of beakers. Then, the solutions were shaked for 20.0 min. After dye extraction, MNPs were quickly separated from the sample solution using a magnet. Desorption process was performed with 2.0 ml of 0.03 M SDS in 0.1 M hydrochloric acid and 2.0 ml of pure acetic acid for Fe_3O_4@SiO_2 and Fe_3O_4@SiO_2-CPTS, respectively. Then, the absorbance of the eluted solutions were measured spectrophotometrically at 617 and 615 nm for Fe_3O_4@SiO_2 and Fe_3O_4@SiO_2-CPTS, respectively, against the reagent blank and plotted versus the concentration of MG in the sample before contacting with MNPs.

Preparation of Fish Samples [44]

Trout were obtained from a local market. The fish samples were filleted and the bones were removed. A volume equivalent to 50 ml of ethanol 10% was added to

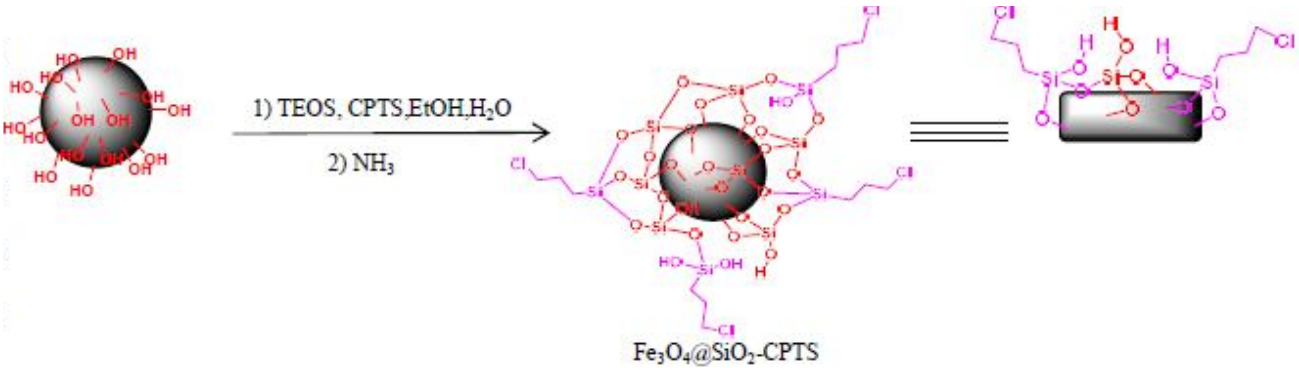

Fig. 1. Preparation process of CPTS-SiO_2 supported on superparamagnetic Fe_3O_4 nanoparticle.

28.33 g of fish tissue. Then, after ultrasonic extraction for 30 min, the mixture was filtered and 5 ml of NaOH 1 M was added for removal of fatty acids. After centrifugation, the upper layer was separated and passed through an oxidation column containing PbO_2. By passing the sample through the PbO_2 column, LMG is oxidized to MG. Then, pH of the sample was adjusted by hydrochloric acid and sodium hydroxide. The resultant sample was analyzed based on the procedure explained in "Analytical procedure".

Preparation of Bottom Sediment of Fish Farming Pool

The water samples were firstly filtered through a Whatman filter paper. Their pH was adjusted to the optimal value by addition of hydrochloric acid and sodium hydroxide.

For the analysis of the sediment, an amount equivalent to 1263.5 g of the sediment was dissolved in 500 ml of deionized water. Then, it was filtered through a Whatman filter paper. The filtrate was centrifuged for 30 min and the upper solution was filtered again. For adjusting pH, solutions of hydrochloric acid and sodium hydroxide were used. The above samples were then analyzed based on the procedure explained in "Analytical procedure".

RESULTS AND DISCUSSIONS

Characterization of the Synthesized MNPs

FTIR study. The functionalities on the surface of MNPs can be confirmed through FTIR spectra. FTIR spectrum of Fe_3O_4@SiO_2-CPTS is shown in Fig. 2. The absorption band at 1100 cm^{-1} is shifted to 1050 and the band at 1010.1 cm^{-1} is shifted to 1300 cm^{-1} due to Si-O-Si and Si-O-Fe [45]. The characteristic absorption band of Fe-O bond is at 576 cm^{-1}. The vibration of OH is observed at 3434 cm^{-1}.

The FTIR spectrum of Fe_3O_4@SiO_2 was recorded and is shown in Fig. 3. The spectrum shows the core shell of the particles with Si-O on the surface. The broad peak at 3447 cm^{-1} could be related to the vibration of OH [46]. The bands at 1083, 800 and 452 cm^{-1} are attributed to the asymmetric Si-O-Si stretching vibration, the symmetric Si-O-Si stretching vibration and the O-Si-O shearing vibration, respectively [47,48]. The bands around 1000 cm^{-1} have been assigned to the asymmetric Fe-O-Si stretching vibration [47,49]. These results suggested that the Fe-SiO_2 interaction exists in the MNP in the form of Fe-O-Si structure. The band at 551 cm^{-1} can be assigned to the Fe-O stretching in Fe-O-Si bonds [46].

Scanning electron microscopy (SEM). To reveal the fine details of the structure of the synthesized MNPs, SEM study was performed. The SEM images of the synthesized Fe_3O_4@SiO_2-CPTS and Fe_3O_4@SiO_2 are shown in Fig. 4 and Fig. 5, respectively. As seen in Figs. 4 and 5, the particle sizes are about 100 nm and smaller. From the SEM analysis, it is found that there are holes and cave type openings on the surface of the adsorbent providing more accessible surface area for adsorption.

X-Ray diffraction. XRD pattern of the synthesized MNPs are shown in Figs. 6 and 7 for Fe_3O_4@SiO_2 and Fe_3O_4@SiO_2-CPTS, respectively. The phases identified based on the XRD studies for the samples are cubic

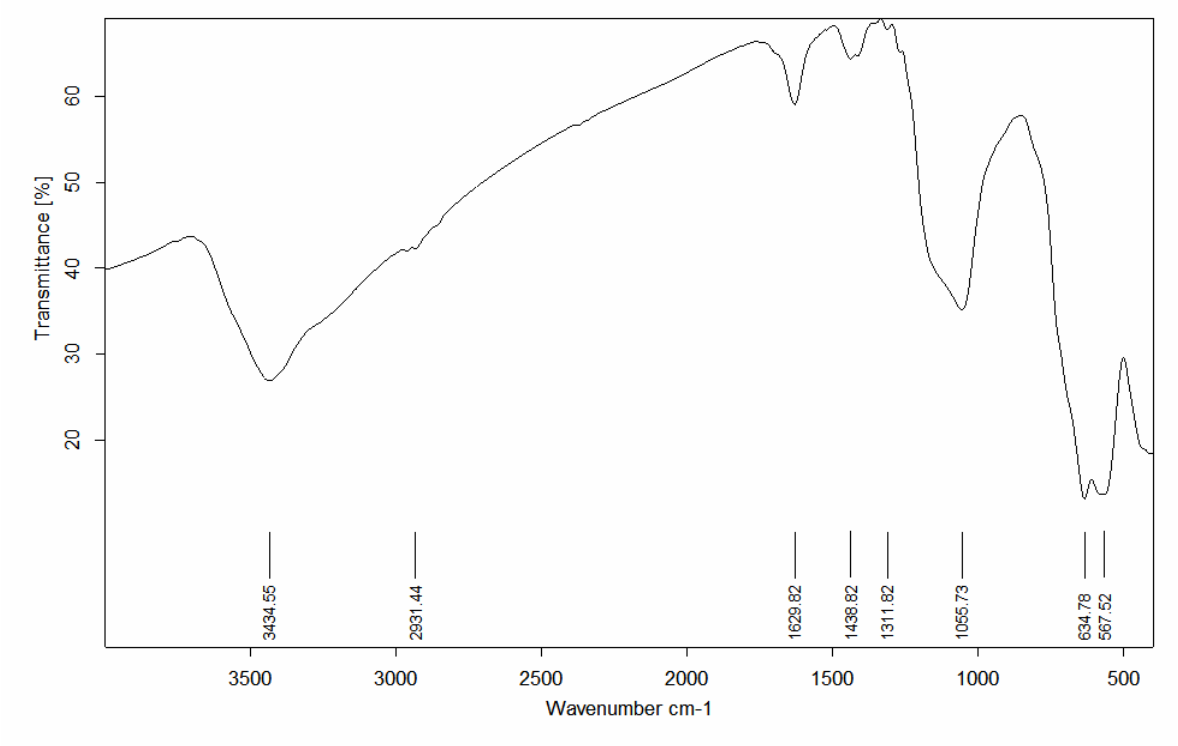

Fig. 2. FT-IR spectrum of CPTS-SiO_2@Fe_3O_4.

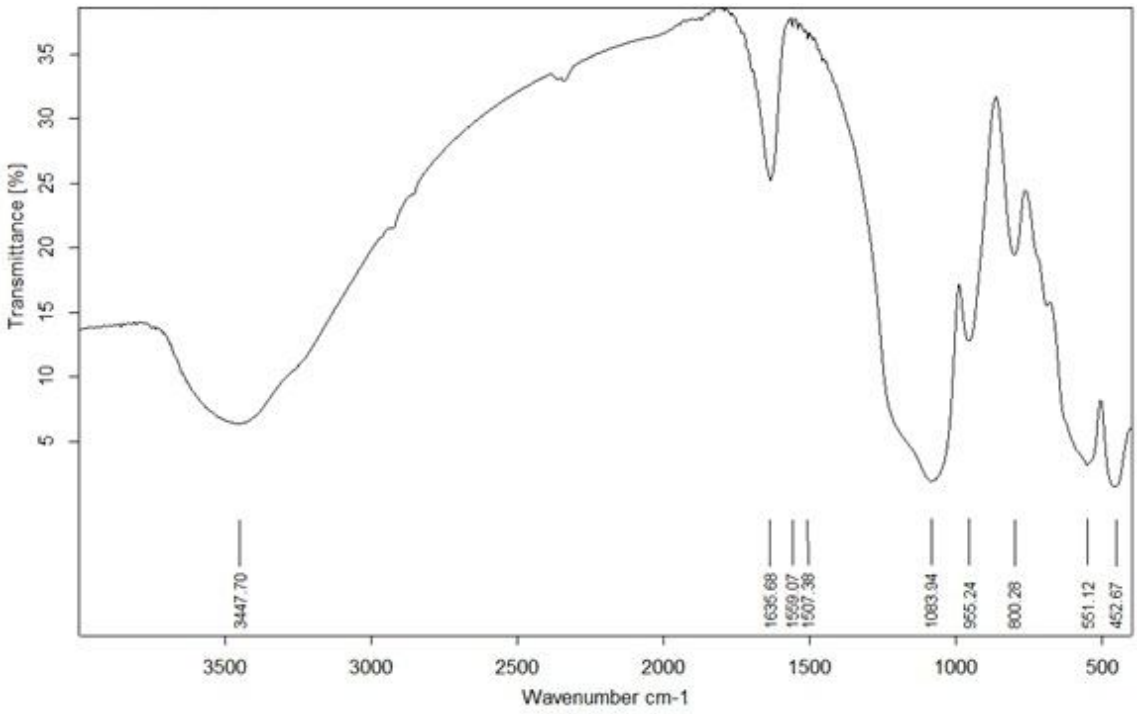

Fig. 3. The FTIR spectrum of SiO_2@Fe_2O_3.

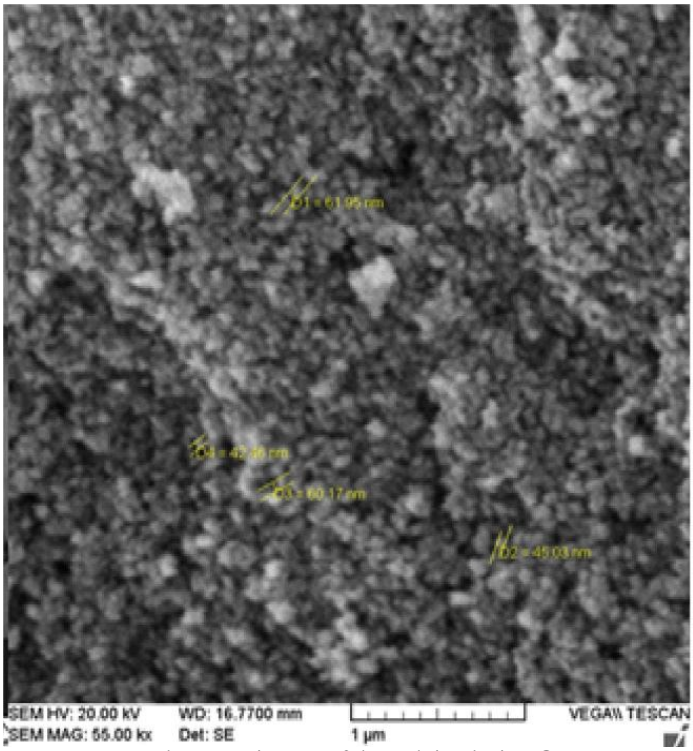

Fig. 4. The SEM image of the calcined SiO_2@Fe_2O_3.

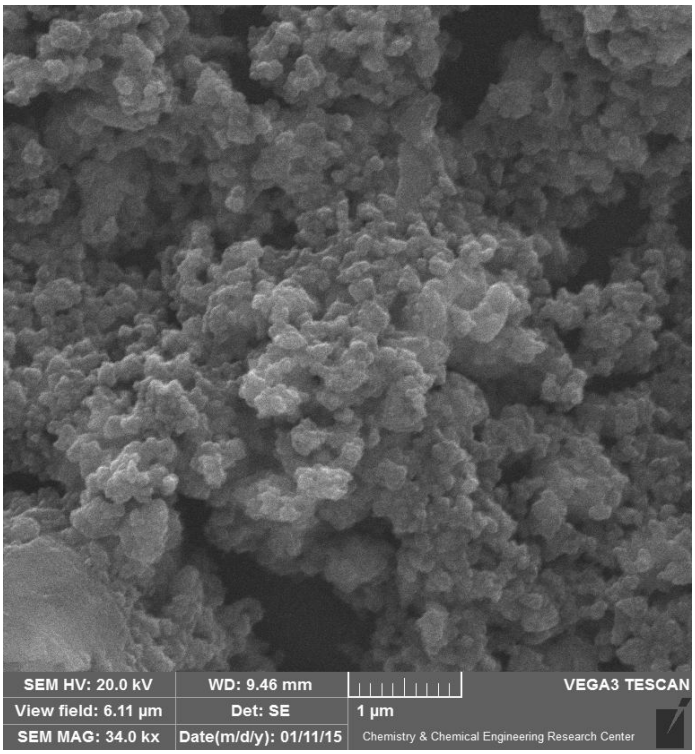

Fig. 5. SEM image of the synthesized Fe_3O_4@SiO_2-CPTS nanoparticle.

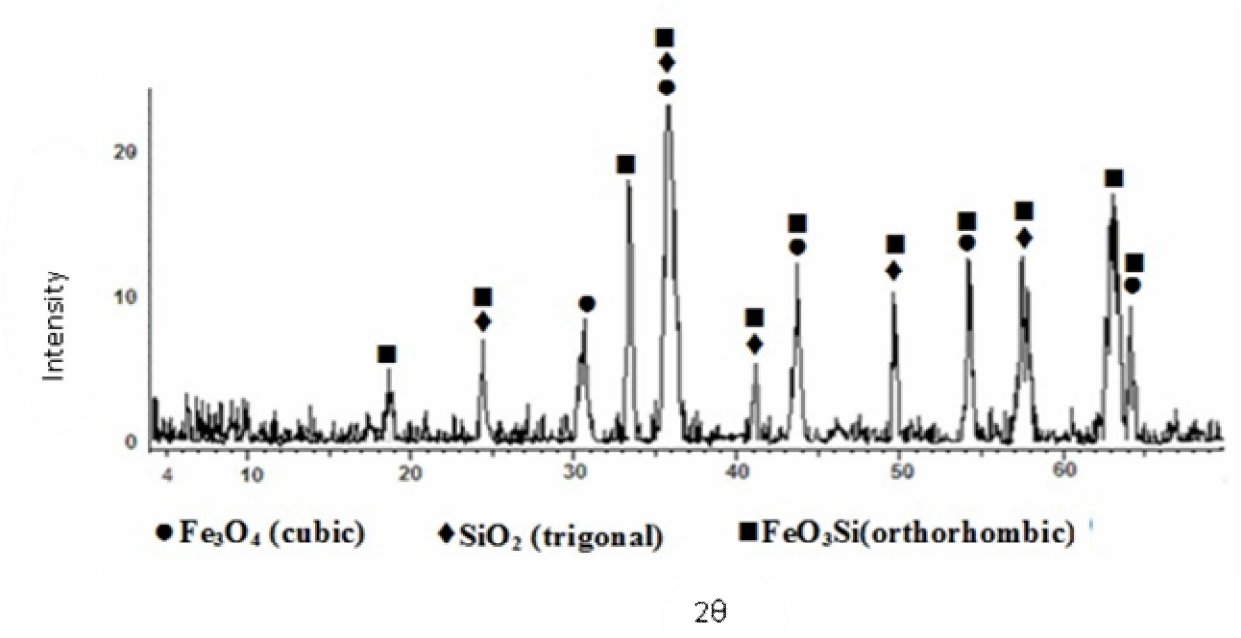

Fig. 6. XRD pattern of the magnetic SiO_2@Fe_2O_3.

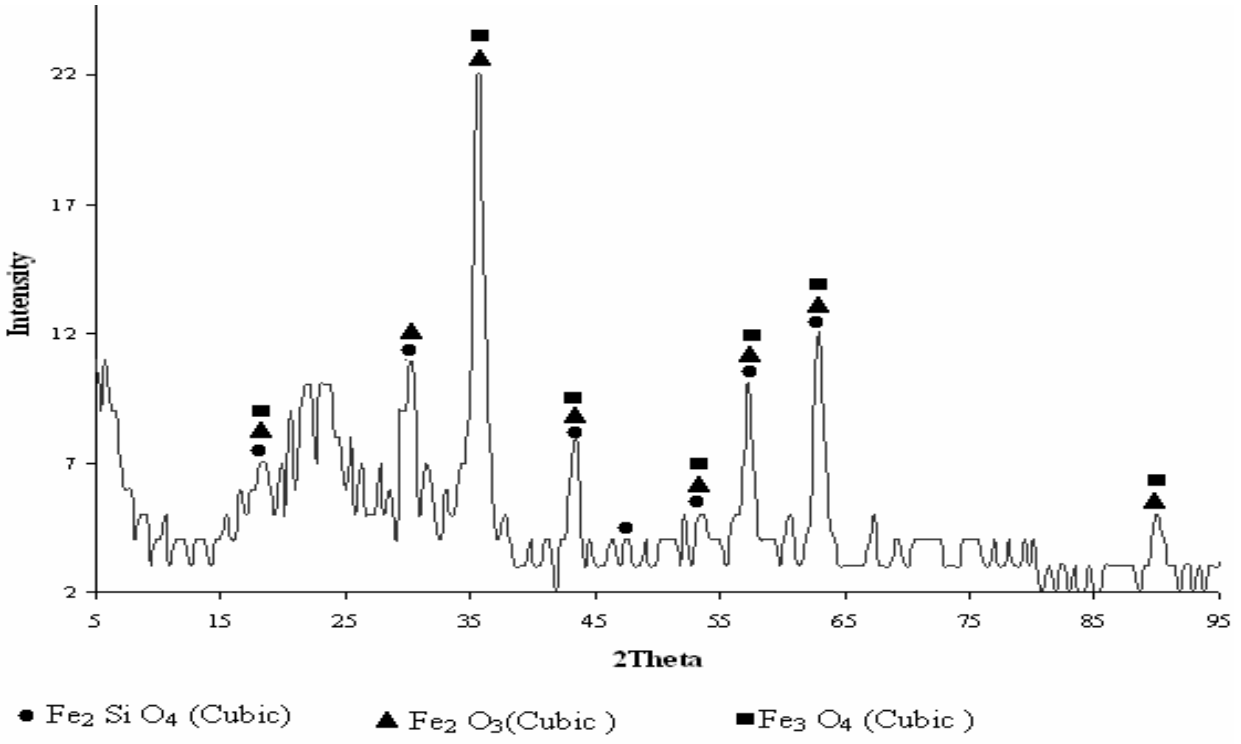

Fig. 7. XRD pattern of the synthesized Fe_3O_4@SiO_2-CPTS nanoparticle.

Fe_2SiO_4, Fe_3O_4 and Fe_2O_3.

Average width of all major peaks in XRD pattern was used for calculation of the crystallite size of the synthesized sample by Debye-Scherrer Eq. [50]:

$$Dc = k\lambda/(\beta\cos\theta) \quad (1)$$

where β is the width of the observed diffraction line at its half maximum intensity, k is the so-called shape factor which usually takes a value of about 0.9, and λ is the wavelength of the X-ray source used in the XRD. Using the above equation, the mean crystallite size (Dc) of the Fe_3O_4@SiO_2 and Fe_3O_4@SiO_2-CPTS was calculated to be 29.7 nm and 48 nm, respectively.

Vibrating sample magnetometry (VSM). In order to show the maintenance of magnetic properties of Fe_3O_4@SiO_2 after functionalization with CTPS, VSM of Fe_3O_4@SiO_2-CPTS was recorded and shown in Fig. 8. The saturation magnetization of Fe_3O_4@SiO_2-CPTS was found to be 47 emu g^{-1}, which is a high magnetic property.

Response Surface Methodology

Response surface methodology (RSM) is a combination of mathematical and statistical techniques followed by determination of optimal region which allows the determination and evaluation of the relative significance of parameters, even in the presence of interactions [51]. In this method, modeling is performed by fitting first or second order polynomials equations to the experimental responses obtained in the experimental design, followed by analysis of variance (ANOVA). The validated model can be plotted in tridimensional graph. This gives a response surface which corresponds to the desired response function and can be used to identify the best operating conditions of the process. Here, central composite design (CCD) was used for designing experiments as a RSM.

CCD is well suited for fitting a quadratic surface, which usually works well for the process optimization [48]. CCD involves the following steps: performing the statistically designed experiments according to the design, selection of factors and levels; and estimating the coefficients of the mathematical model based on the experimental responses to predict the response and check its adequacy [51,52]. In CCD, it is assumed that the central point for each factor is zero and the design is symmetrical around it [51]. Factors influencing the studied systems are amount of MNPs (x_1), pH (x_2) and time (x_3) for Fe_3O_4@SiO_2, and amount of MNPs (x_1) and pH (x_2) for Fe_3O_4@SiO_2-CPTS. Since adsorption of MG onto Fe_3O_4@SiO_2-CPTS was relatively fast, time was not considered as a factor for adsorption studies by this MNP. With these factors, 20 and 13 experiments were designed for adsorption of MG by Fe_3O_4@SiO_2 and Fe_3O_4@SiO_2-CPTS, respectively (Tables S1 and S2). Responses of the experiments have also been included in Tables S1 and S2. Concentration of MG in these experiments is 4.00 mg l^{-1}.

The following equation was used to calculate the dye adsorption efficiency (response) in the experiments:

$$Y\% = 100 \times (C_i - C_r)/C_i \quad (2)$$

where C_i and C_r are the initial and residual concentration of the dye in the solution, respectively. ANOVA of the performed experiments (Tables S1 and S2) is given in Tables 1 and 2.

The results of the ANOVA for Fe_3O_4@SiO_2 (Table 1) shows that among the linear terms, x_1 is a significant factor in adsorption of MG at 95% confidence level (p value calculated for this factor has been smaller than 0.05 and corresponding F statistics is high (10.51)). However, pH (x_2) is also is relatively important factor for adsorption of MG onto this MNP (p = 0.073).

For Fe_3O_4@SiO_2-CPTS (Table 2), square term of pH ($x_2 \times x_2$) is significant at 95% confidence level. As can be inferred from ANOVA table (Table 2), amount of Fe_3O_4@SiO_2-CPTS (x_2) is not significant at the 95% confidence level. This is because of the efficient adsorption of dye by Fe_3O_4@SiO_2-CPTS. Interaction between the studied factors is not important for the studied MNPs. This can be realized from the p value calculated for the terms $x_1 \times x_2$, $x_1 \times x_3$ and $x_2 \times x_3$ for Fe_3O_4@SiO_2 and $x_1 \times x_2$ for Fe_3O_4@SiO_2-CPTS in Tables 1 and 2.

Based on the statistic analysis of the designed experiments, the following response equations were used to correlate the dependent and independent variables for Fe_3O_4@SiO_2 and Fe_3O_4@SiO_2-CPTS MNPs, respectively.

$$Y = B_0 + B_1x_1 + B_2x_2 \quad (3)$$

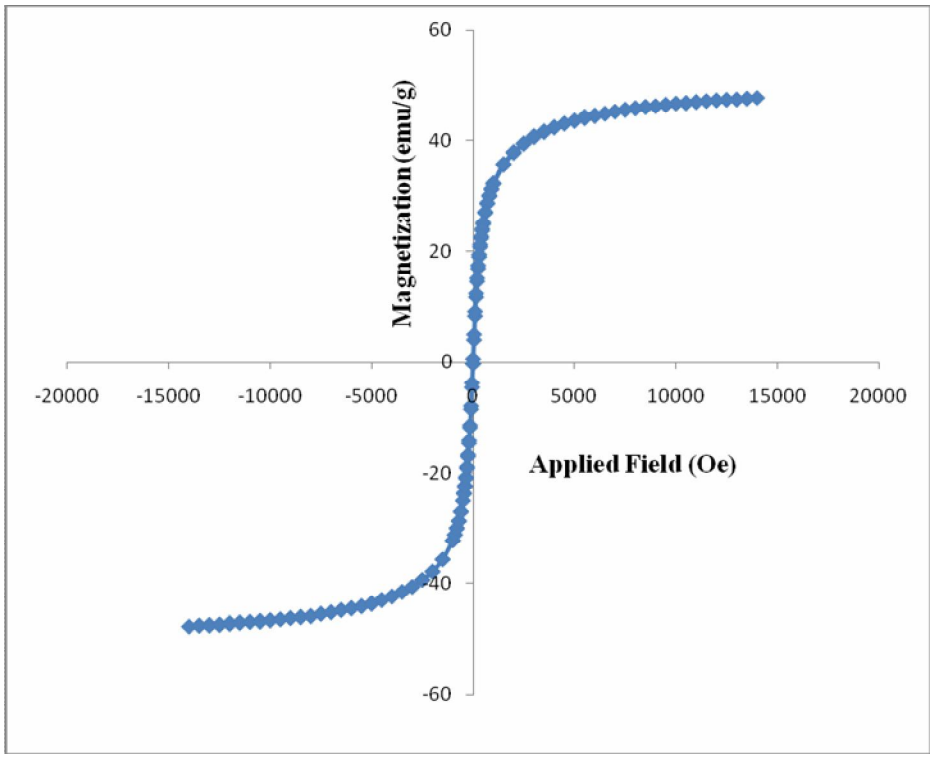

Fig. 8. VSM curve of the synthesized Fe_3O_4@SiO_2-CPTS magnetic nanoparticle.

Table 1. Results of ANOVA for the Experiments and Responses Reported in Table S1 for Fe_3O_4@SiO_2. Variables x_1, x_2 and x_3 are mg of MNP, pH and Time, Respectively

Term	Coefficient	p^a	F^b
Constant	74.996	0.000	
x_1	13.915	0.009	10.51
x_2	8.586	0.073	4.00
x_3	5.814	0.205	1.83
$x_1 \times x_1$	-4.496	0.595	0.30
$x_2 \times x_2$	-1.861	0.825	0.05
$x_3 \times x_3$	7.259	0.396	0.79
$x_1 \times x_2$	-2.776	0.576	0.33
$x_1 \times x_3$	-4.366	0.384	0.83
$x_2 \times x_3$	-5.296	0.296	1.22
Regression		0.121	2.17
R%	66.18		

[a]Probability value. [b]F statistics.

Table 2. Results of ANOVA for the Experiments and Responses Reported in Table S2 for Fe_3O_4@SiO_2-CPTS. Variables x_1 and x_2 are mg of MNP and pH, Respectively

Term	Coefficient	p^a	F^b
Constant	97.1020	0.000	
x_1	1.5559	0.366	0.93
x_2	0.9968	0.556	0.38
$x_1 \times x_1$	-0.1485	0.934	0.01
$x_2 \times x_2$	-6.5110	0.007	14.21
$x_1 \times x_2$	-2.3275	0.341	1.04
Regression		0.073	3.35
R%	70.50		

[a]Probability value. [b]F statistics.

$$Y = B_0 + B_{22}x_2x_2 \quad (4)$$

where, Y is the response, B_0 is constant, B_1, B_2 and B_{22} are regression coefficients for linear effect of x_1, linear effect of x_2, and quadratic coefficient for x_2, respectively.

The dye adsorption efficiencies (Y) have been predicted by Eqs. (3) and (4) and presented in Tables S1 and S2 for Fe_3O_4@SiO_2 and Fe_3O_4@SiO_2-CPTS, respectively. The results indicate a good agreement between the experimental and predicted values of the adsorption efficiency. The results of the ANOVA showed that the regression model had a satisfactory value of coefficient of determination (R^2 = 66.18 and 70.50) for Fe_3O_4@SiO_2 and Fe_3O_4@SiO_2-CPTS, respectively. This implies that 66.18% and 70.50% of the variations of the adsorption efficiency are explained by the factors for Fe_3O_4@SiO_2 and Fe_3O_4@SiO_2-CPTS, respectively.

In the next step of design, response surfaces were plotted based on Eqs. (3) and (4). Figures 4 and 5 represent the relevant fitted response surfaces for the designs. These plots were obtained for a given pair of factors at central value of other variables. As can be seen in Figs. 9 and 10, in higher amounts of MNPs (x_1), the response (Adsorption%) is higher. For Fe_3O_4@SiO_2, in higher pHs (x_2), the adsorption is also favored (see Figs. 4a and 4b). However, for Fe_3O_4@SiO_2-CPTS, intermediate pHs are more suitable for adsorption of MG (see Fig. 10). Moreover, a high curvature of response surface with change in the level of pH (x_2) can be seen for Fe_3O_4@SiO_2-CPTS (see Fig. 10). The significance of this curvature can also be inferred from the p value of the term $x_2 \times x_2$ in Table 2 ($p < 0.05$). As expected, the higher is shaking time (x_3), the higher is response (see Fig. 9c). The increased percentage of adsorption of MG was observed with increase in pH.

Adsorption increases by increasing pH and reaches a maximum at pH about 5.8 for Fe_3O_4@SiO_2-CPTS and decreases at higher pH values. The decrease in adsorption with decrease in pH in two MNPs can be simply justified. As pH of the system decreases, the number of positively charged surface sites increases, this does not favor the adsorption of positively charged dye cation due to electrostatic repulsion. Moreover, the lower adsorption of MG at acidic pH can be due to the presence of the excess H^+ ions competing with dye cations for the adsorption sites of MNPs. As the pH further increases, the adsorption decreases for Fe_3O_4@SiO_2-CPTS. This can be related to the neutral form of MG in these pHs which is favorite for adsorption onto the surface of Fe_3O_4@SiO_2-CPTS which is insensitive to pH (see Fig. 1). However, for Fe_3O_4@SiO_2, increasing pH favors the adsorption probably by changing

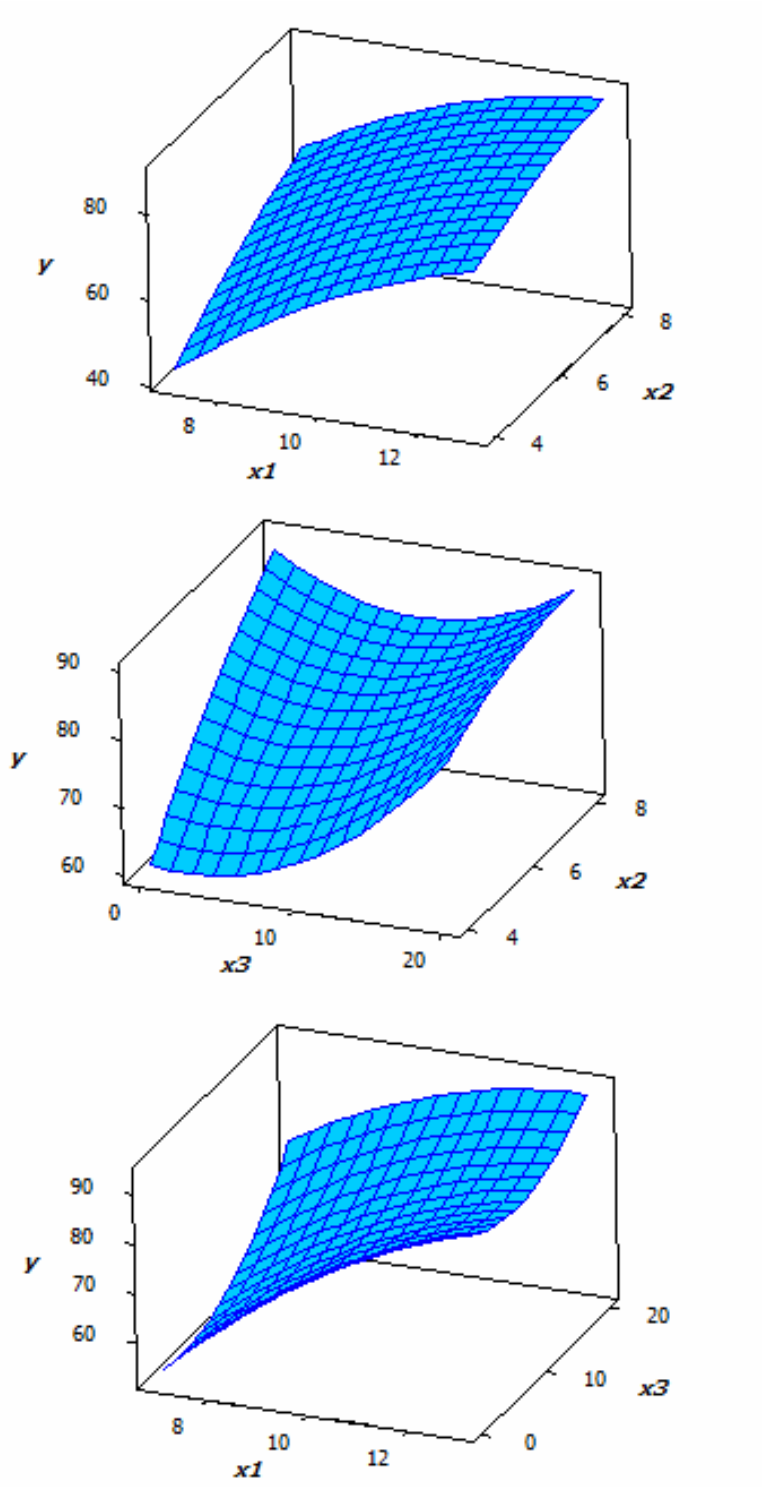

Fig. 9. Response surfaces obtained by the model with coefficients reported in Table 1 for (a) x_1 (mg of Fe_3O_4@SiO_2) and x_2 (initial pH), (b) x_3 (time) and x_2 (initial pH) and (c) x_1 (mg of Fe_3O_4@SiO_2) and x_3 (time).

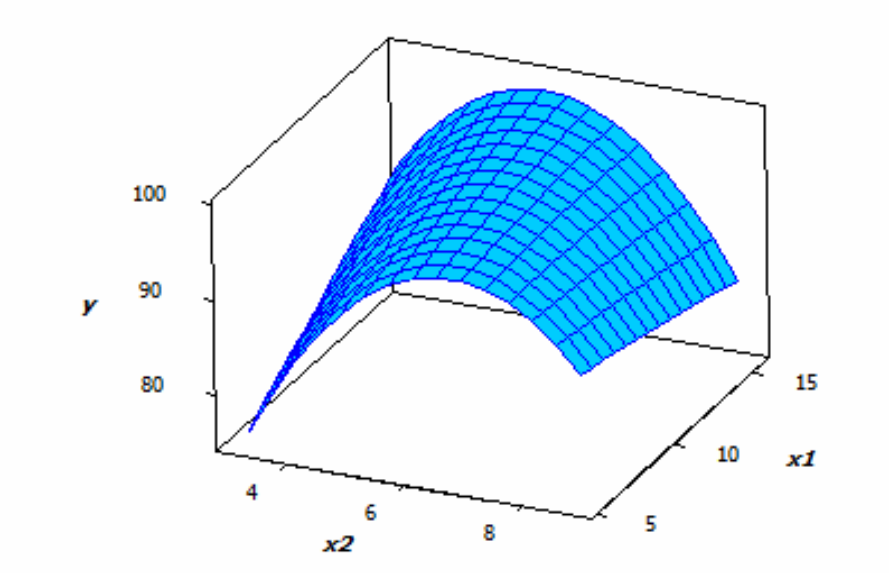

Fig. 10. Response surface obtained by the model with coefficients reported in Table 2 for x_1 (mg of Fe_3O_4@SiO_2-CPTS) and x_2 (initial pH).

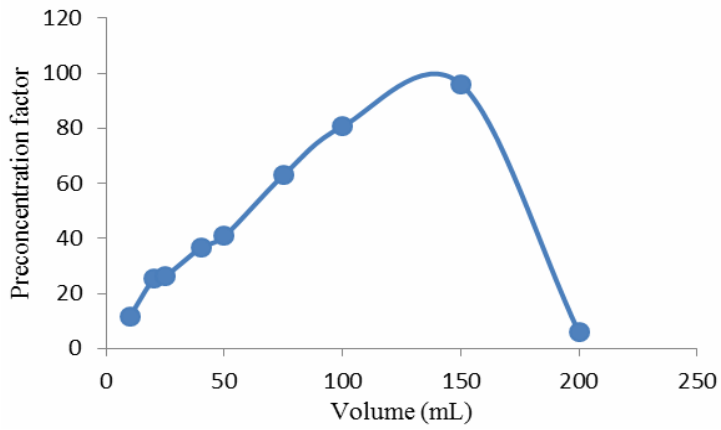

Fig. 11. Effect of sample volume on the adsorption of MG onto the surface of Fe_3O_4@SiO_2-CPTS (15.5 mg) in pH 5.8.

the surface charges from positive to negative [15]. It is known that pH can affect the structural stability of MG and consequently its color intensity [53]. The pK_a value for MG is 6.9 and in aqueous solutions, it can occur in two cationic and colorless carbinol forms [54].

Adsorption Studies

Effect of sample volume. It is important to determine the maximum volume of the sample which can be introduced to the sorbent without a considerable loss in adsorption efficiency. The value of this volume is a function of the analyte retention on the particular sorbent and can be only altered by a change of sorbent and depends on the parameters such as adsorbent amounts and bed thickness. Here, effect of sample volume on the adsorption of MG was studied in the range 10-250 ml. In order to study the effect of sample volume, 4.0 ml of 10.0 mg l^{-1} MG was diluted to 10.0, 20.0, 25.0, 40.0, 50.0, 75.0, 100.0, 150.0, 200.0

and 250.0 ml with deionized water. Then, adsorption and desorption processes were performed under the optimal pH 5.8 using 15.5 mg Fe_3O_4@SiO_2-CPTS as described in experimental section. For Fe_3O_4@SiO_2, the preconcentration factor of 5 was obtained (volume of sample equivalent to 10 ml). The result for Fe_3O_4@SiO_2-CPTS is shown in Fig. 11. As can be seen from Fig. 11, adsorption increases up to the volume of 150 ml. However, in larger volumes, it decreases. Therefore, for determination of trace quantities of MG in real samples, a sample volume of 150.0 ml for Fe_3O_4@SiO_2-CPTS can be selected in order to achieve the maximum preconcentration factor.

Adsorption isotherms. Analysis of isotherm data is important for predicting the adsorption capacity of the adsorbent which is one of the main parameters required for the design of an adsorption system. The equilibrium adsorption isotherm is fundamental in describing the behavior between adsorbate and adsorbent [41].

Equilibrium isotherm studies were carried out with different initial concentrations of MG (1.0-50.0 mg l^{-1}) at pH values of 8.0 and 5.8 for Fe_3O_4@SiO_2 and Fe_3O_4@SiO_2-CPTS, respectively in 25 ºC. The Langmuir model [55] was used to analyze the equilibrium adsorption data. Langmuir isotherm describes nonlinear balance between the amount of analyte adsorption and release to the solution at a constant temperature. The general form of the Langmuir isotherm is:

$$\frac{q_e a_L}{K_L} = \frac{K_L C_e}{1 + K_L C_e} \tag{5}$$

where C_e is the equilibrium concentration (mg l^{-1}) of MG in the solution in contact with MNP, and q_e is the amount of MG adsorbed per unit mass of the adsorbent (mg g^{-1}) at equilibrium concentration. C_e, a_L (l mg^{-1}) and K_L (l g^{-1}) are the Langmuir constants. a_L is related to the adsorption energy and $q_{max} = [K_L/a_L]$ signifies the maximum adsorption capacity (mg g^{-1}) which depends on the number of adsorption sites. The linear form of Langmuir's isotherm is given by the following equation:

$$\frac{C_e}{q_e} = \left(\frac{C_e}{q_{max}}\right) + \left(\frac{1}{K_L q_{max}}\right) \tag{6}$$

where, q_{max} (mg g^{-1}) is the maximum amount of adsorption of adsorbent as mono layer. The values of a_L and K_L are calculated from the slope and intercept of the plot C_e/q_e *versus* C_e. The amount of MG adsorbed (mg g^{-1}) was calculated based on a mass balance equation as given below:

$$q_e = \frac{V(C_0 - C_e)}{W} \tag{7}$$

where C_0 is the initial concentration of MG in mg l^{-1}, V is the volume of the solution in l, and W is the dry weight of nanoparticles in g [47]. The essential feature of the Langmuir isotherm can be expressed in terms of a dimensionless constant separation factor (R_L) given by the following equation:

$$R_L = \frac{1}{1 + a_L C_0} \tag{8}$$

The value of R_L indicates the type of isotherm: irreversible ($R_L = 0$), linear ($R_L = 1$), unfavorable ($R_L > 1$) or favorable ($0 < R_L < 1$) [56]. The R_L value for Fe_3O_4@SiO_2 and Fe_3O_4@SiO_2-CPTS in the present study were calculated and are given in Table 3. As can be inferred from data in Table 3, the adsorption of the MG on to the studied MNPs is favorable ($0 < R_L < 1$) . Also, the parameters of the Langmuir isotherm were calculated and are given Table 3.

Data in Table 3 indicates that q_{max} for Fe_3O_4@SiO_2 and Fe_3O_4@SiO_2-CPTS is 22.172 and 25.70 mg g^{-1}, respectively, and the values of correlation coefficient, *r*, for the fit of experimental data to Langmuir isotherm is close to 1.00. The interpretability of the experimental data by Langmuir isotherm (Figs. S1 and S2) suggests that adsorption of MG is limited to monolayer coverage and the surface is relatively homogenous in terms of functional groups with significant interaction with MG molecules

The q_{max} for the adsorption of MG on the Fe_3O_4@SiO_2 and Fe_3O_4@SiO_2-CPTS is listed in Table 4 along with the literature values obtained by other adsorbents [11,40,50,57-70]. As is evident from data in Table 4, adsorption capacity of the studied MNPs, in most case, is comparable with the reported values.

Table 3. Parameters of Langmuir Isotherm for the Adsorption of MG on Fe_3O_4@SiO_2 and Fe_3O_4@SiO_2-CPTS at 25 ºC in Optimal Conditions

	a_L (l mg^{-1})	K_L (l g^{-1})	$q_{max} = [K_L/a_L]$ (mg g^{-1})	Concentration of MG (mg l^{-1})	R_L	r
Fe_3O_4@SiO_2-CPTS	0.6626	1.4692	22.172	5.0	0.7513	0.9984
Fe_3O_4@SiO_2	0.02855	0.7339	25.70	5.0	0.8750	0.9909

Table 4. Comparison of MG Adsorption Capacity of Fe_3O_4@SiO_2 and Fe_3O_4@SiO_2-CPTS with other Adsorbents

Type of adsorbent	q_{max} (mg g^{-1})	Ref.
Neem sawdust	4.354	[57]
Cellulose	2.422	[58]
Activated charcoal	0.18	[59]
Arundo donax root carbon (ADRC)	8.49	[60]
Bentonite	7.72	[61]
Bentonite ($Cd(OH)_2$-NW-AC)	7.72	[62]
Fe_3O_4@Mel	9.06	[40]
Caulerpa racemosavar.cylindracea (CRC)	25.67	[62]
Lemon peel	51.73	[63]
Jute fiber carbon	136.59	[64]
Polymeric gels	4.9	[65]
Sugar cane dust	4.88	[66]
Brown-rotted pine wood	42.43	[67]
Sea shell powder	42.33	[68]
Eucalyptus bark	59.88	[53]
Iron humate	19.2	[69]
Hen feathers	26.1	[11]
EDTAD-modified sugarcane bagasse	157.2	[70]
Activated carbons commercial grade (ACC)	8.27	[60]
Fe_3O_4@SiO_2	22.17	Present work
Fe_3O_4@SiO_2-CPTS	25.70	Present work

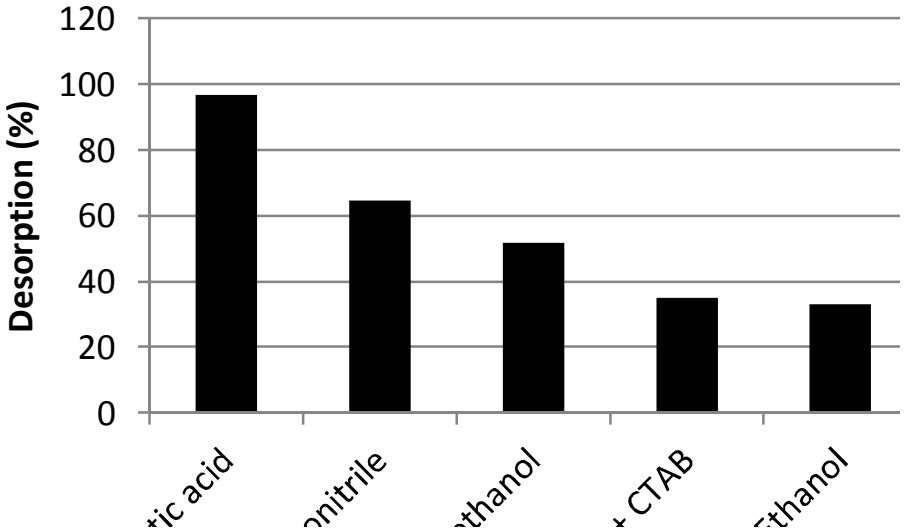

Fig. 12. The recovered MG percent in desorption by different eluents for Fe_3O_4@SiO_2 (a) and Fe_3O_4@SiO_2-CPTS (b).

Table 5. Statistical Results of the Calibration of MG by the Proposed Method Based on the Adsorption and Preconcentration by Fe_3O_4@SiO_2-CPTS

Parameters	Characteristic
λ_{max} (nm)	615
Molar absorptivity (M^{-1} cm^{-1})	1187234.1
Linear range (mg l^{-1})	0.01-15.00
Intercept of calibration curve	1.2574
Slope of calibration curve	3.4575
Standard error of intercept	0.2900
t statistics of intercept	4.33
Standard error of slope	0.0602
Standard error of regression	1.01
t statistics of slope	57.43
Correlation coefficient	0.9955
Detection limit (DL)[a] (mg l^{-1})	2.00×10^{-4}

[a]Calculated DL = (3Sb/m) where DL, Sb, m are the limit of detection, standard deviation of the blank and the slope of the calibration graph, respectively.

Desorption of MG

Different eluents were investigated for desorbing MG from MNPs. Desorption process was performed on loaded MNPs in optimal conditions. MG loaded adsorbent was washed by 2.0 ml of different eluents. Figure 12 shows the percentage of the recovered dye after elution by different eluents. The figures show that 2.0 ml of SDS 0.03 M in hydrochloric acid and glacial acetic acid are the best eluents for desorption of MG from Fe_3O_4@SiO_2 and Fe_3O_4@SiO_2-CPTS, respectively. By these eluents, 94.17% and 96% of the adsorbed MG onto surface of Fe_3O_4@SiO_2 and Fe_3O_4@SiO_2-CPTS can be desorbed, respectively. The results of the study of the reusability of the Fe_3O_4@SiO_2-CPTS have been reported in supplementary materials.

Analytical Data

Increasing concentrations of MG were contacted with Fe_3O_4@SiO_2 and Fe_3O_4@SiO_2-CPTS in optimal extraction conditions and then, MG was desorpted by 2.0 ml of 0.03 M solution of SDS in 0.1 M HCl and glacial acetic acid, respectively.

For constructing calibration curve, the spectrophotometric signal of the solution obtained by desorption process was plotted against the concentration of MG. The calibration curve was linear in concentration ranges of 0.7-14.0 mg l^{-1} at wavelength 617 nm for Fe_3O_4@SiO_2 and in the range of 0.01-15.0 mg l^{-1} at wavelength 615 nm for Fe_3O_4@SiO_2-CPTS. Statistical parameters of the calibration curves were calculated and reported in Table S4 and Table 5 for Fe_3O_4@SiO_2 and Fe_3O_4@SiO_2-CPTS, respectively.

The high value of the molar absorptivity and the low value of DL show the high sensitivity of method based on the adsorption and preconcentration by Fe_3O_4@SiO_2-CPTS. Using the Fe_3O_4@SiO_2-CPTS, the slope of the calibration curve has increased about 24 times compared toFe_3O_4@SiO_2. Therefore, the method is more sensitive using this MNP. The standard errors of the parameters of calibration are also significantly low. Moreover, the linearity of the calibration curve is validated by the high value of the correlation coefficient (which were close to unity) of the calibration curve. The dynamic linear range of the calibration with Fe_3O_4@SiO_2-CPTS is very wide (more than three orders of magnitude). Therefore, the method can be applied to determine MG in different samples with a wide variation in concentration of the analyte. Sensitivity of the proposed method based on the extraction and preconcentration by Fe_3O_4@SiO_2-CPTS is clearly inferred from the high slope of the calibration curve, lower limit of the dynamic linear range and DL.

Application to Real Samples

The chemical matrix effect is characterized by dependence of the sensitivity on the sample matrix composition. This effect can be detected by comparing the slope of the calibration curves corresponding to pure standards with the slope of the standard addition line in different real samples. Significant difference of the two slopes shows the presence of matrix effect in the analyzed sample.

For investigation of matrix effect, five standards were added to each real sample and extraction by Fe_3O_4@SiO_2-CPTS was performed. After desorption, the spectra were recorded and absorbances at 615 nm were plotted versus the added concentrations. Slopes of the standard addition lines were 3.6561, 3.2821 and 3.7247 for fish farming water, bottom sediment of fish farming pool and fish tissue, respectively. Clearly, these slopes are numerically different from that obtained for standards in Table 5 (3.4575). For a close and logical comparison, *t* test was performed for identification of the significance of the difference between slopes in real samples and calibration with standards. Calculated *t* statistics are 2.23, 1.25 and 2.32 for fish farming water, bottom sediment of fish farming pool and fish tissue, respectively. Critical *t* value at 95% confidence level with 4 degrees of freedom is 2.78. Therefore, it can be concluded that there is not a significance difference between the slopes in real samples and slope of the calibration with standards and consequently, matrix effect is absence. So, Fe_3O_4@SiO_2-CPTS can effectively separate and extract MG from complex matrices.

In order to assess the analytical applicability of the proposed method, it was applied to determine MG in different samples by Fe_3O_4@SiO_2 and Fe_3O_4@SiO_2-CPTS. The results are summarized in Table 6. The data obtained indicates that the percent relative error (RE%) and percent

Table 6. Results Determination of MG in Different Samples Based on the Adsorption and Preconcentration by Fe_3O_4@SiO_2 and Fe_3O_4@SiO_2-CPTS

Real sample	Added concentration (mg l^{-1})	Predicted concentration (mg l^{-1})[a]	Recovery (%)	RE%	RSD%
	SiO_2@Fe_2O_3				
Aquarium water 1	0.0	0.806[a]			
	2.0	2.805[a]	97.23	-2.7	5.2
Aquarium water 2	0.0	1.102[a]			
	2.0	3.078[a]	98.13	-1.86	2.1
	CPTS-SiO_2@Fe_3O_4				
Fish tissue	0.00	1.711 (mg kg^{-1})[a]			
	2.00	136.330 (mg kg^{-1})	92.9	-9.5	2.6
Bottom sediment of fish farming pool	0.00	2.342 (mg kg^{-1})[b]			
	2.00	163.430 (mg kg^{-1})	98.8	-1.1	2.7
Fish farming water	0.00	0.279[b]			
	2.00	2.266	99.4	-0.6	0.4

a) Mean of five determinations. b) Mean of three determinations.

relative standard deviation (RSD%) values are satisfactory. Very low percent relative errors indicate that the method is selective. In addition, the data clearly showed that the Fe_3O_4@SiO_2-CPTS can effectively extract MG in complex matrices. A good agreement was obtained between the added and measured analyte amounts. The sensitivity and selectivity of the proposed method enables its application to determine MG in fish tissue samples. In the proposed method, Fe_3O_4@SiO_2-CPTS can extract MG in the complex fish tissue matrix and pure acetic acid can effectively elute the extracted MG from Fe_3O_4@SiO_2-CPTS.

a) Mean of five determinations.
b) Mean of three determinations.

Comparison with the Reported Methods

The main characteristics of the reported methodologies [36,40,71-75] for the determination of MG in fish and water samples have been collected in Tables 7 and S5, respectively. The linear range of the method presented here is satisfactory and relatively wide. The upper limit of the linear range of the proposed method is higher than other methods. The high values of molar absorptivity and low values of DL indicate the high sensitivity of the proposed method. The values of RSD% and RE% of the proposed method are low. As can be inferred from data in Table 7, comparable analytical characteristics have been reported using complicated methods and expensive instruments such as HPLC, MS, isotope dilution and Rayleigh scattering.

CONCLUSIONS

In this work, Fe_3O_4@SiO_2-CPTS was synthesized as a novel magnetic adsorbent for adsorption, preconcentration and determination of MG in various samples. The adsorption process followed Langmuir isotherm suggesting that the adsorption on the surface of Fe_3O_4@SiO_2-CPTS occurred as a monolayer. A high preconcentration factor for

Table 7. Reported Results for Determination of MG in Fish Samples

Instrumental methodology		Determination range ($mg\ l^{-1}$)	DL ($mg\ l^{-1}$)	Recovery (%)	RSD%	Samples	Ref.
Isotope dilution liquid Chromatography/mass spectrometry (ID-LC/MS)		0.8-18.0 ($\mu g\ kg^{-1}$)	0.02 ($\mu g\ kg^{-1}$)	50-80		Salmon tissue	[71]
HPLC-VIS detection after immunoaffinity column clean-up		0.3×10^{-3}-1.5×10^{-2}	0.15 ($ng\ g^{-1}$)	88	5.4	Fish tissue	[72]
Bilinear model	RBL algorithm			81.9-101.1%	2.1-5.3	Fish tissue	
	U-PLS/RBL algorithm			81.5-100.4%	2.6-5.2		[73]
Resonance rayleigh scattering spectra method and non-linear scattering spectra method	RRS method	0.1×10^{-3}-1.2×10^{-2}	3.7×10^{-3}				
	SOS method	0.6×10^{-3}-0.01	1.8×10^{-3}			Fish tissue	[74]
	FDS method	0.9×10^{-3}-0.01	2.7×10^{-2}				
Melamine supported magnetic iron oxide nanoparticles (Fe3O4@Mel) for spectrophotometric determination		0.1×10^{-3}-8×10^{-3}	0.05×10^{-3}	90.0	<1.66	Fish tissue	[40]
DWO–RRS methods		5×10^{-3}-6	1.5×10^{-3}	97.5	1.8	Fish tissue	[75]
Liquid chromatography with visible and fluorescence detection		0-10^{-5}	1.041×10^{-5}	62	<10.9	Carp muscle	[36]
Fe_3O_4@SiO_2-CPTS		0.01-15	$2/0002 \times 10^{-4}$	90/45	-9/54	fish tissue	Present work

MG was obtained using Fe_3O_4@SiO_2-CPTS. The method is simple, precise, sensitive and highly efficient for preconcentration and determination of MG that can be applied to analyze the real samples.

REFERENCES

[1] S. Srivastava, R. Sinha, D. Roy, Aquatic Toxicol. 66 (2004) 319.

[2] A. Albert, Selective Toxicology, 6th ed., Chapman & Hall London, 1979.
[3] A. Swarbrick, E.J. Murby, P. Hume, J. Liq. Chromatogr. Related Technol. 20 (1997) 2269.
[4] M.M.A. Hussein, S. Wada, K. Hatai, A. Yamamoto, Antimicotic Activity of Eugenol against some Water Molts. Symposium on Diseases in Asian Aquaculture, Philippines, 1999.
[5] T.A. Qureshi, R. Chauhan, Y. Prasad, S.A. Mastan, J. Ecotoxicol. Environ. Monitoring 8 (1998) 2.
[6] F.J. Foster, L. Woodbury, Prog. Fish-Culturist 3 (1936) 7.
[7] C. Long, Z. Mai, B. Zhu, X. Zou, Y. Gao, X. Huang, J. Chromatogr. A 1203 (2008) 21.
[8] A. Stammati, C. Nebbia, I.D. Angelis, A.G. Albo, M. Carletti, C. Rebecchi, F. Zampaglioni, M. Dacasto, Toxicol. *In vitro* 19 (2005) 853.
[9] N. Littlefield, B.N. Blackwell, C.C. Hewitt, D.W. Gaylor, Toxicol. Sci. 5 (1985) 902.
[10] B. Samiey, A. Raoof Toosi, J. Hazard. Mater. 184 (2010) 739.
[11] A. Mittal, J. Hazard. Mater. 133 (2006) 196.
[12] C. Directive, 2002/657/EC Commission Decision of 12 August 2002, Implementing Council Directve 96/23/EC, Brussels, Off. J. Eur. Commun. L2002, 221, 8.
[13] L. Valle, C. Díaz, A.L. Zanocco, P. Richter, J. Chromatogr. A 1067 (2005) 101.
[14] M. Maier, H. Fritz, M. Gerster, J. Schewitz, E. Bayer, Anal. Biochem. 262 (1998) 177.
[15] H.H. Yang, S.Q. Zhang, X.-L. Chen, Z.-X. Zhuang, J.-G. Xu, X.-R. Wang, Anal. Chem. 76 (2004) 1316.
[16] A. Sergi, F. Shemirani, M. Alvand, A. Tajbakhshian, Anal. Methods 6 (2014) 7744.
[17] M. Babazadeh, R. Hosseinzadeh-Khanmiri, J. Abolhasani, E. Ghorbani-Kalhor, A. Hassanpour, RSC Adv. 5 (2015) 19884.
[18] Q.G. Liao, L.F. Hu, L.G. Luo, Anal. Methods 7 (2015) 2806.
[19] S. Ata, M. Berber, H. Çabuk, M. Akyüz, Anal. Methods 7 (2015) 6231.
[20] R. Mohammad-Rezaei, H. Razmi, V. Abdollahi, A.A. Matin, Anal. Methods 6 (2014) 8413.
[21] S.-N. Xu, Q. Zhao, H.-B. He, B.-F. Yuan, Y.-Q. Feng, Q.-W. Yu, Anal. Methods 6 (2014) 7046.
[22] J. Abolhasani, R. Hosseinzadeh Khanmiri, E. Ghorbani-Kalhor, A. Hassanpour, A.A. Asgharinezhad, N. Shekari, A. Fathi, Anal. Methods 7 (2015) 313.
[23] A.E. Chávez-Guajardo, J.C. Medina-Llamas, L. Maqueira, C.A.S. Andrade, K.G.B. Alves, C.P. de Melo, Chem. Engin. J. 281 (2015) 826.
[24] H. Hosseinzadeh, S. Mohammadi, Carbohyd. Polym. 134 (2015) 213.
[25] Y. Wang, Y. Zhang, C. Hou, Z. Qi, X. He, Y. Li, Chemosphere 141 (2015) 26.
[26] M. Oplatowskaa, L. Connollya, P. Stevenson, S. Stead, C.T. Elliott, Anal. Chim. Acta 698 (2011) 51.
[27] M.-C. Yang, J.-M. Fang, T.-F. Kuo, D.-M. Wang, Y.-L. Huang, L.-Y. Liu, P.-H. Chen, T.-H. Chang, J. Agr. Food Chem. 55 (2007) 8851.
[28] W. Xing, L. He, H. Yang, C. Sun, D. Li., X. Yang, Y. Li, A. Deng, J. Sci. Food Agr. 89 (2009) 2165.
[29] L. An, J. Deng, L. Zhou, H. Li, F. Chen, H. Wang, Y. Liu, J. Hazard. Mate. 175 (2010) 883.
[30] J.L. Allen, J.R. Meinertz, J. Chromatogr. A 536 (1991) 217.
[31] K. Mitrowska, A. Posyniak, J. Zmudzki, J. Chromatogr. A 1089 (2005) 187.
[32] L.G. Rushing, E.B. Hansen, J. Chromatogr. B: Biomed. Sci. Appl. 700 (1997) 223.
[33] W.C. Andersen, S.B. Turnipseed, C.M. Karbiwnyk, R.H. Lee, S.B. Clark, M.R. Rowe, W.D. Madson, K.E. Miller, Anal. Chim. Acta 637 (2009) 279.
[34] W.C. Andersen, S.B. Turnipseed, J.E. Roybal, LIB No 4363, U.S. Food and Drug Administration 21 (2005) 1.
[35] M.D. Hernando, M. Mezcua, J.M. Súarez-Barcena, A.R. Fernández-Alba, Anal. Chim. Acta 562 (2006) 176.
[36] M.J.M. Buenoa, S. Herreraa, A. Uclés, A. Agüera, M. Dolores Hernando, O. Shimelis, M. Rudolfsson, A.R. Fernández-Alba, Anal. Chim. Acta 665 (2010) 47.
[37] Y.J. Xu, X.H. Tian, X.Z. Zhang, X.H. Gong, H.H. Liu, H.-J. Zhang, H. Huang, L.-M. Zhang, J. Chromatogr. Sci. 50 (2012) 591.
[38] Y.F. Tao, D.M. Chen, X.Q. Chao, H. Yu, P. Yuanhu, Z. Liu, L. Huang, Y. Wang, Z. Yuan, Food Control 22

(2011) 1246.
[39] S.B. Turnipseed, W.C. Andersen, J.E. Roybal, J. AOAC Int. 88 (2005) 1312.
[40] R. Mirzajani, S. Ahmadi, Industrial and Engin. Chem. Res. 23 (2015) 117.
[41] A. Afkhami, R. Moosavi, T. Madrakian, Talanta 82 (2010) 785.
[42] I. Simkiene, M. Treideris, G. Niaura, R. Szymczak, P. Aleshkevych, A. Reza, I.K. Salynas, V. Bukauskas, G.J. Babonas, Mater. Chem. Phys. 130 (2011) 1026.
[43] W. Wu, Q. He, C. Jiang, Nanosc. Res. Let. 3 (2008) 397.
[44] L. Luo, Y. Yang, Q. Wang, Z. Luo, Z. Qu, Z. Yang, Microchem. J. 132 (2017) 100.
[45] K. Wapner, G. Grundmeier, Surf. Coat. Tech. 200 (2005) 100.
[46] D. Predoi, O. Crisan, A. Jitianu, MC. Valsangiacom, M. Raileanu, M. Crisan, M. Zaharescu, Thin Solid Films 515 (2007) 6319.
[47] S. Bruni, F. Cariati, M. Casu, A. Lai, A. Musinu, G. Piccaluga, S. Solinas, Nanostruct. Mater. 11 (1999) 573.
[48] S. Bordiga, R. Buzzoni, F. Geobaldo, C. Lamberti, E. Giamello, A. Zecchina, G. Leofanti, G. Petrini, G. Tozzola, G. Vlaic, J. Catal. 158 (1996) 486.
[49] P. Fabrizioli, T. Bürgi, M. Burgener, S. van Doorslaerb, A. Baiker, J. Mater. Chem. 12 (2002) 619.
[50] H.P. Klug, L.E. Alexander, X-ray Diffraction Procedures for Polycrystalline and Amorphous Materials, 2nd ed., Wiley, New York, 1974.
[51] R.H. Myers, D.C. Montgomery, Response Surface Methodology: Process and Product Optimization Using Designed Experiments. 2nd ed.; John Wiley and Sons: New York, 2002.
[52] R.G. Brereton, Chemometrics: Data Analysis for the Laboratory and Chemical Plant, John Wiley, 2003, pp. 76-84.
[53] S. Chowdhury, P. Saha, Chem. Engin. J. 164 (2010) 168.
[54] S.J. Culp, F.A. Beland, Int. J. Toxicol. 15 (1996) 219.
[55] L. Langmuir, J. Am. Chem. Soc. 40 (1918) 1361.
[56] G. McKay, H.S. Blair, J.R. Gardner, J. Appl. Polym. Sci. 27 (1982) 3043.
[57] S.D. Khattri, M.K. Singh, J. Hazard. Mater. 167 (2009) 1089.
[58] C.P. Sekhar, S. Kalidhasan, V. Rajesh, N. Rajesh, Chemosphere 77 (2009) 842.
[59] M.J.I Qbal, M.N. Ashiq, J. Hazard. Mater. 139 (2007) 57.
[60] J. Zhang, Y. Li, C. Zhang, Y. Jing, J. Hazard. Mater. 150 (2008) 774.
[61] S.S. Tahir, N. Rauf, Chemosphere 63 (2006) 1842.
[62] Z. Bekci, Y. Seki, L. Cavas, J. Hazard. Mater. 161 (2009) 1454.
[63] K.V. Kumar, Dyes and Pigments 74 (2007) 595.
[64] K. Porkodi, K. Vasanth Kumar, J. Hazard. Mater. 143 (2007) 311.
[65] M.A. Malana, S. Ijaz, M.N. Ashiq, Desalination 263 (2010) 249.
[66] S.D. Khattri, M.K. Singh, Adsorpt. Sci Technol. 17 (1999) 269.
[67] H. Zhang, Y. Tang, X. Liu, Z. Ke, X. Su, D. Cai, X. Wang, Y. Liu, Q. Huang, Z. Yu, Desalination 274 (2011) 97.
[68] S. Boutemedjet, O. Hamdaoui, Desalination and Water Treatment 8 (2009) 201.
[69] P. Janos, Environ. Sci. Technol. 37 (2003) 5792.
[70] Y. Xing, D. Deng, Sep. Sci. Technol. 44 (2009) 2117.
[71] S. Ahn, B. Kim, Y. Lee, J. Kim, Bull. Korean Chem. Soc. 31 (2010) 3228.
[72] J. Xie, D.-D. Chen, Q.-J. Zhang, G.-M. Wang, X. Wang, Q. Guo, F. Jiang, D. Chen, J. Deng, J. Chromatogr. B 913- 914 (2013) 123.
[73] J.-T. Yuan, L.-F. Liao, X.-L. Xiao, B. He, S.-Q. Gao, Food Chem. 113 (2009) 1377.
[74] Y. Song, S. Liu, Z. Liu, X. Hu, Spectrochim. Acta Part A: Mol. Biomol. Spectroscopy 78 (2011) 148.
[75] J. Zhu, M. Qin, S. Liu, Z. Liu, J. Yang, X. Hu, Spectrochim. Acta Part A: Mol. Biomol. Spectroscopy 130 (2014) 90.